A new anisotropic soft tissue model for elimination of unphysical auxetic behaviour

B. Fereidoonnezhad[a], C. O'Connor[a], J. P. McGarry[a,*]

[a]*Biomedical Engineering, National University of Ireland Galway, Galway, Ireland*

Abstract

Auxetic behaviour , the unphysical transverse expansion during uniaxial tension, is a common and undesirable feature of classical anisotropic hyperelastic constitutive models for soft tissue. In this study we uncover the underlying mechanism of such behaviour; high levels of in-plane compaction occurs due to increasing tension in strain-stiffening fibres, leading to unphysical out-of-plane expansion. We demonstrate that auxetic behaviour is primarily influenced by the ratio of fibre to matrix stiffness, and is accentuated by strain-stiffening fibres in a constant stiffness matrix (e.g., the widely used neo-Hookean matrix with exponentially stiffening fibres). We propose a new bilinear strain stiffening fibre and matrix (BLFM) model which allows close control of the fibre-matrix stiffness ratio, thereby robustly eliminating auxetic behaviour. We demonstrate that our model provides accurate prediction of experimentally observed out-of-plane compaction, in addition to stress-stretch anisotropy, for arterial tissue subjected to uniaxial tension testing.

Keywords: Hyperelasticity, Constitutive modeling, Anisotropy, Soft tissue, Auxetic behaviour, Strain-stiffening fibre-matrix model

1. Introduction

The hyperelastic strain energy density function used to model fibrous soft tissues is typically decomposed into an anisotropic part (representing the contribution of aligned families of fibres), and an isotropic part (representing the contribution of non-fibrous ground matrix). Common examples include models of arterial tissue (Gasser et al., 2006; Nolan and McGarry, 2016a; Fereidoonnezhad et al., 2016; Holzapfel et al., 2015), cartilage (Dowling et al., 2013; Brown et al., 2009; Pierce et al., 2013; Deneweth et al., 2015), and the annulus fibrosis (Guo et al., 2006; Peng et al., 2006). The most commonly imple-

*Corresponding author

Email address: patrick.mcgarry@nuigalway.ie (J. P. McGarry)

mented form for the strain energy density function entails exponentially strain-stiffening fibres in parallel with a near-linear neo-Hookean ground matrix, following from the work of Holzapfel, Gasser and Ogden (2000). While such an additive decomposition of soft tissue stress into a fibre contribution and a ground matrix contribution is attractive in terms of physical interpretation of the constitutive law, auxetic behaviour (i.e. orthogonal expansion during uniaxial tension) is a common and undesired feature of such models (Skacel and Bursa, 2016, 2019; Volokh, 2017). To better illustrate such auxetic behaviour , we reproduce a simulation from the '*Abaqus benchmarks Guide*' (input file *adventitia_circ.inp*) of uniaxial tension of an adventitial strip cut along circumferential direction (Abaqus, 2017). The material is modelled using the well-known HGO constitutive model (Gasser et al., 2006), with fibre families prescribed at $\pm 49.98\,^{\circ}$, as shown in Figure 1A. As shown in Figure 1 thickness in the out-of-plane 3-direction increases as the specimen is stretched. While auxetic behaviour has been reported for certain classes of synthetic materials (e.g. foams and lattice materials (Lim, 2015)), such auxetic behaviour is not observed in experimental tests of artery tissue (Skacel and Bursa, 2016). To the best of the authors knowledge, auxetic behaviour has not been reported in any naturally occurring soft tissue or tissue engineered collagen constructs. Therefore, in the context of soft tissue material models, we refer to the computation of auxetic behaviour as unphysical.

Auxetic behaviour of soft tissue hyperlastic models has been the subject of three recent studies. Skacel and Bursa (2016) demonstrated the computation of auxetic behaviour (which they refer to as a negative Poisson's ratio) for the anisotropic hyperelastic soft tissue models of Holzapfel et al. (2000) and Gasser et al. (2006; 2012). The authors incorrectly suggest that such unphysical auxetic response might be the result of model incompressibility. In a follow-on study the authors later demonstrate that introduction of volumetric compressibility into constitutive model in fact increases auxetic behaviour of the models (Skacel and Bursa (2019)). The recent study by Volokh (2017) considers an anisotropic hyperelastic model with exponential stiffening and fibre dispersion. The author suggested that a more accurate consideration of the fibre dispersion could be used to reduce the auxetic effect. Fibre dispersion is also taken into account in the models investigated by Skacel and Bursa (Skacel and Bursa, 2016, 2019). However, in Section 7 of the current study, we demonstrate that dispersion can merely reduce, but not eliminate, auxetic behaviour. Furthermore, fibre disperion is a physically motivated model feature

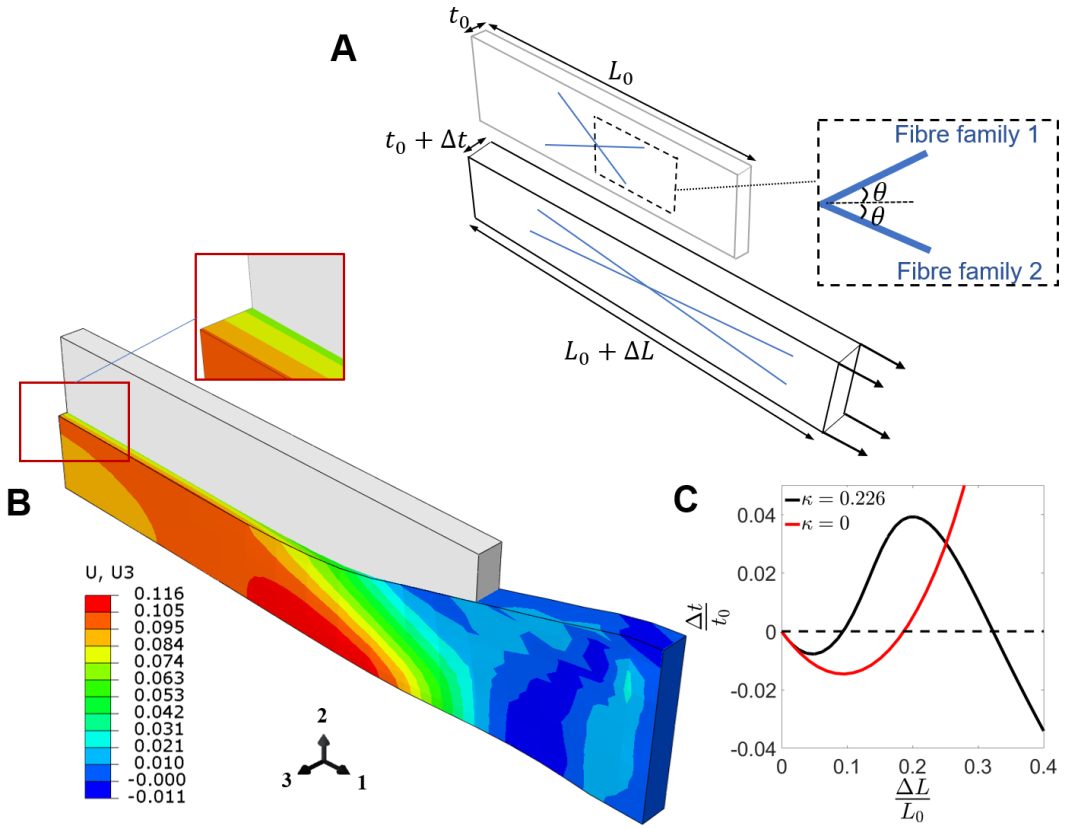

Figure 1: Results of the *Abaqus Benchmark Guide* example Abaqus (2017) for uniaxial tension of an adventitial strip cut along the circumferential direction. (A) Two fibre families oriented as $\theta = \pm 49.98\ ^{\circ}$are considered. (B) Increase in the thickness of the strip in the case of fully aligned fibres ($\kappa = 0$) at $\frac{\Delta L}{L_0} = 0.33$. (C) An increase in the thickness of the strip is computed for $\frac{\Delta L}{L_0} > 0.2$ in the case of fully aligned fibres ($\kappa = 0$) and for $0.09 < \frac{\Delta L}{L_0} < 0.3$ in the case of dispersed fibres ($\kappa = 0.226$) . The reader is refer to Abaqus (2017) for details of material parameters and dimensions.

that must be calibrated to reproduce observed material anisotropy. It is therefore not an independent parameter that can be used to control auxetic behaviour.

The three previous studies (Skacel and Bursa, 2016, 2019; Volokh, 2017) demonstrate that incorrect computation of auxetic behaviour is a general problem for established anisotropic hyperelastic soft tissue models. However, these studies do not uncover the underlying mechanistic cause of such auxetic behaviour, but merely focus on secondary factors such as compressiblity and fibre dispersion. No study to date has uncovered the root cause of computed auxetic behaviour in anisotropic soft tissue models, and no study has proposed a robust solution for such incorrect behaviour.

The current paper (i) provides, for the first time, an explanation for the underlying

mechanism of auxetic behaviour in anisotropic soft tissue models, and (ii) proposes a new constitutive law for anisotropic soft tissue that robustly controls and eliminates auxetic behaviour. The paper is structured as follows. In Section 2 we provide a mechanistic explanation for the computation of auxetic behaviour in fibre reinforced soft tissue models. In Section 3 we demonstrate the key role of the fibre-matrix stiffness ratio in auxetic behaviour. In Section 4 we demonstrate that strain stiffening fibres in a constant stiffness matrix promotes auxetic behaviour at high strains. In Section 5 we propose a novel bilinear strain stiffening fibre and matrix model (BLFM model) and we demonstrate that this new formulation allows robust control of out-of-plane deformation and elimination of auxetic behaviour, resulting in accurate prediction of experimentally measured artery anisotropic strain stiffening and out-of-plane contraction.

2. Why does auxetic behaviour occur?

In order to provide a clear explanation of the origin of auxetic behaviour for constitutive models of fibrous tissue, we consider the simple case of a cube that consists of a matrix material and two families of embedded collagen fibres. Following the typical approach for artery models, we assume that the fibres are confined to the (1-2) plane and are symmetric about the 1-direction (see Figure 1A). Following the established approach for the modelling of hyperelastic soft tissue, the strain energy density function is additively decomposed into an isotropic matrix contribution and an anisotropic fibre contribution:

$$\Psi = \Psi_m + \Psi_f \tag{1}$$

This leads to an additive decomposition of the Cauchy stress tensor:

$$\sigma_i = \sigma_i^m + \sigma_i^f \tag{2}$$

Therefore, when the cube is subjected to uniaxial tension in the 1-direction, the equilibrium equations in the 2- and 3-directions can be written as:

$$\begin{aligned} \sigma_2 &= \sigma_2^m + \sigma_2^f = 0, \\ \sigma_3 &= \sigma_3^m + \sigma_3^f = \sigma_3^m = 0 \end{aligned} \tag{3}$$

where σ_2^m and σ_3^m are the 2- and 3-components of the matrix Cauchy stress tensor, respectively. σ_2^f is the 2-component of the fibre Cauchy stress tensor. Because we assume

that fibres are confined to the (1-2) plane without any out-of-plane contribution, σ_3^f is equal to zero. Additionally, due to symmetry of the two fibre families about the loading direction, the 1-, 2-, and 3-direction are the principal directions. Typically the constitutive law for fibres assume significant strain stiffening (e.g. exponential stiffening of collagen fibres) whereas matrix constitutive laws typically assume much lower strain stiffening (e.g. neo-Hookean model without progressive stiffening). Therefore, when a high level of stretching is imposed on the cube in the 1-direction, the fibres exert significant tension in the 2-direction (in addition to a larger contribution in the 1-direction). Therefore, to achieve stress equilibrium, the near constant stiffness matrix must develop large negative strains in the 2-direction such that $\sigma_2^m = -\sigma_2^f$. As a result of extreme matrix compaction in the 2-direction, the matrix may undergo expansion in the 3-direction in order to satisfy stress equilibrium. Such expansion in a lateral direction during uniaxial stretching is referred to as auxetic behaviour. Such behaviour is not observed experimentally for arterial tissue (Skacel and Bursa, 2016), or, to our knowledge, any other soft tissue. Therefore, new modelling strategies to control and eliminate the computation of non-physical auxetic behaviour must be developed for anisotropic fibrous soft tissue.

3. The simple case of linear fibres in a linear matrix

We begin our investigation with a simple parametric analysis of the sensitivity of auxetic behaviour to (i) fibre to matrix stiffness ratio, (ii) fibres orientation and (iii) matrix compressibility. In this Section we initially limit our analysis to linear fibre and linear matrix behaviour in order to elucidate the factors underlying auxetic behaviour. Once again, a cube with two fibre families confined to the (1-2) plane is considered, with applied uniaxial extension in the 1-direction (Figure 2).

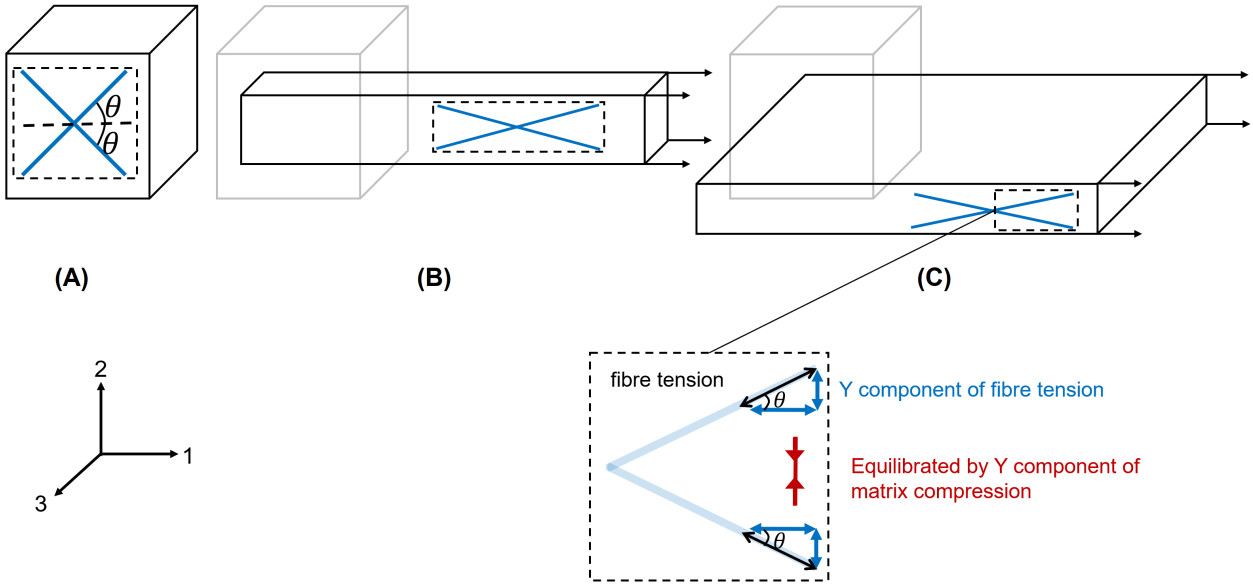

Figure 2: Schematic of the uniaxial tension of a fibre-reinforced cube with two fibre families. (a) undeformed cube (b) deformed cube without auxetic behaviour , and (c) deformed cube with auxetic behaviour . The fibres are distributed in (1-2) plane.

Hyperelastic constitutive models for arterial tissue and other fibrous soft tissues are defined through the strain energy density function Ψ as follows:

$$\Psi(\mathbf{C}, \mathbf{a}_{0i}) = \Psi_m(\mathbf{C}) + \sum_{i=4,6} \Psi_{fi}(\mathbf{C}, \mathbf{a}_{0i}) \tag{4}$$

$\Psi_m(\mathbf{C})$ and $\Psi_{fi}(\mathbf{C}, \mathbf{a}_{0i})$ are the strain energy density contributions of the ground matrix and collagen fibres, respectively. Two fibre families ($i = 4, 6$) are represented in equation (4), as commonly assumed for arterial tissue. $\mathbf{C} = \mathbf{F}^{\mathrm{T}}\mathbf{F}$ is the right Cauchy–Green tensor, where $\mathbf{F}$ is the deformation gradient tensor. Typically for soft tissue (e.g. arteries) two fibre families are represented, and $\mathbf{a}_{0i}$ are two fibre directions in the reference configuration. Typically $\Psi_m(\mathbf{C})$ is decomposed into isochoric and volumetric matrix contributions, such that

$$\Psi_m(\mathbf{C}) = \Psi_{\mathrm{vol}}(J) + \overline{\Psi}_m(\overline{\mathbf{C}}). \tag{5}$$

$\overline{\mathbf{C}} = J^{-2/3}\mathbf{C}$ is the isochoric modified right Cauchy–Green tensor, while $J = \det \mathbf{F} > 0$ is the volumetric jacobian. The simple neo-Hookean formulation is generally used to model the ground matrix of soft tissues, such that:

$$\Psi_m(\mathbf{C}) = \frac{K}{2}(J-1)^2 + \frac{\mu}{2}(\bar{I}_1 - 3) \tag{6}$$

where K is the effective bulk modulus and μ is the effective shear modulus. $\bar{I}_1 = \text{tr}\overline{\mathbf{C}}$ is the first invariant of $\overline{\mathbf{C}}$. This formulation provides near-linear stress-strain behaviour. It is convenient to define E_m, the effective matrix stiffness under conditions of uniaxial stress, such that $E_m = 9K\mu/(3K + \mu)$. Note that the volumetric contribution in equation (6) is appropriate for soft tissues that do not undergo large deformations (e.g. arteries (Nolan and McGarry, 2016b)). However, for materials that exhibit large volume changes the reader is referred to Moerman et al. (2020) for more complex volumetric strain energy density functions. For the initial investigation in this section we consider a simplified constant stiffness fibre strain energy density function is given as

$$\Psi_{fi} = E_{1f}(\frac{2}{3}\lambda_{fi}^3 - \lambda_{fi}^2 + \frac{1}{3}) \tag{7}$$

which leads to a linear relationship between fibre Cauchy-stress and fibre stretch, where E_{1f} is the fibre stiffness and λ_{fi} is the fibre stretch obtained as: $\lambda_{fi}^2 = I_i = \mathbf{a}_{0i}.\mathbf{C}\mathbf{a}_{0i}$.

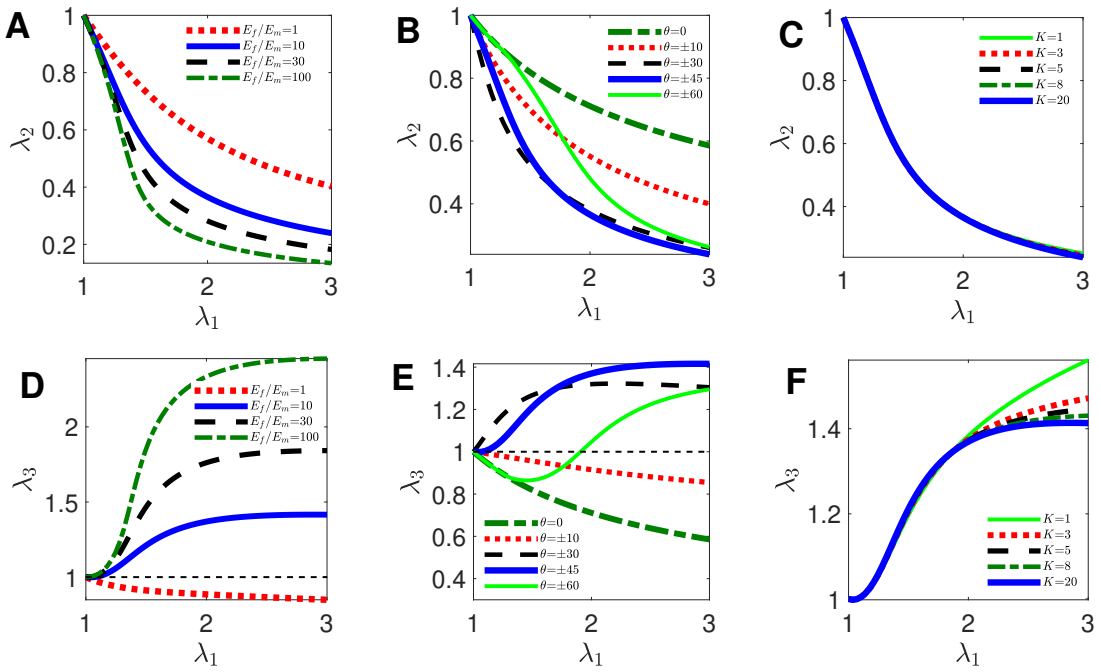

Figure 3: Influence of the fibre to matrix stiffness ratio (A, D), fibre angle (B, E) and compressibility (C, F) on the in-plane (first row) and out-of-plane stretch λ_3 (Second row) for the uniaxial extension of a cubic element of fibrous materials. A neo-Hookean matrix with a linear fibre model with the reference parameters value of $\theta = \pm 45\ ^\circ$, $E_m = 0.5$, $E_f/E_m = 10$ and $K/\mu = 100$ have been used in all plots (blue curves). λ_1 is the stretch in the loading direction.

The results of our initial parameter study for linear fibres in a linear matrix are shown in Figure 3. Computed in-plane contractions λ_2 (Figure 3A, C, E) and the corresponding

out-of-plane deformations λ_3 (Figure 3B, D, F) are plotted as a function of the applied stretch in the x-direction λ_1. $\lambda_3 > 1$ indicates that unphysical auxetic behaviour has been computed. As shown in Figure 3 (A, D), an increase in the fibre to matrix stiffness ratio results in in-plane contraction in the 2-direction, and a corresponding increase in out-of-plane expansion in the 3-direction. Significant auxetic behaviour is computed for all cases in Figure 3, except for the case where the fibre and matrix stiffnesses are equal (i.e. the material is essentially isotropic). In summary, stretching of stiff fibres results in a high component of fibre tension in the 2-direction. Therefore, mechanical equilibrium requires a significant matrix compaction in the 2-direction, with a corresponding matrix expansion in the 3-direction.

Figures 3 B and E show the effect of initial fibre orientation (with respect to the loading direction (1-direction)). As expected, no auxetic behaviour is observed for the case of $\theta = 0\,^\circ$; fibres contribute only to the 11 component of the stress tensor, and the deformation in the 2- and 3-directions is dependent only on the matrix properties. Similarly for the case of $\theta = 10\,^\circ$, fibres are closely aligned to the loading direction and contribute weakly to the 22 component of the stress tensor. Therefore deformations in the 2- and 3- directions are primarily governed by the matrix properties and, again, no auxetic behaviour is computed. For $\theta = 30\,^\circ$auxetic behaviour is computed from the onset of stretching. This occurs due to a high component of fibre tension in the 2-direction. Stress equilibrium therefore results in high matrix compaction in the 2-direction, and consequently an auxetic expansion in the 3-direction. λ_3 is observed to peak at an applied stretch of $\lambda_1 \approx 2$. Further stretching results in further rotation of the fibres towards the loading direction and a consequent slight reduction in λ_3. A similar trend is observed for a fibre angle of $\theta = 45\,^\circ$, with λ_3 peaking at a higher stretch of $\lambda_1 \approx 2.8$.

For fibre angles greater than $\theta = 45\,^\circ$, the fibres are in compression at the start of the deformation. Since fibres are not capable of bearing compressive loads (McEvoy et al., 2018; Holzapfel and Ogden, 2017; Holzapfel and Fereidoonnezhad, 2017), during the initial stages of stretching the material behaves like an isotropic matrix with no fibre contribution and consequently no auxetic behaviour . However, as the deformation increases the fibres rotate towards the stretching (1-) direction and develop a tensile 22-Cauchy stress component. Eventually auxetic behaviour begins to appear and progressively gets worse. The effect of material compressibility on auxetic behaviour is also investigated (Figure 3

C, F). It is observed that auxetic behaviour increases with increasing material compressibility. Figure 3 presents a limited parametric investigation to illustrate the mechanisms underlying auxetic behaviour. It should be noted that the full range of interactions between the governing parameters is not presented. For example, auxetic behaviour will be computed for $\theta = 10\ ^{\circ}$if a fibre to matrix stiffness ratio of $\frac{E_f}{E_m} = 30$ is considered.

4. Auxetic behaviour is increased by strain–stiffening fibres in a linear matrix

The isotropic neo-Hookean model with a linear fibre model has been used for the illustration of the auxetic behaviour and parameter studies in Section 2. However, experimental data of fibrous soft tissue exhibits anisotropic strain-stiffening behaviour . Typically this is captured using a strain-stiffening constitutive model for fibres in parallel with a neo-Hookean matrix.

In order to systematically analyse the role of fibre strain stiffening on auxetic behaviour we propose a new *bilinear strain-stiffening fibre* (BLF) constitutive law. Fibre deformation is considered to consist of three distinct regimes: (i) an initial compliant quasi-linear region to model the stretching of coiled collagen fibres; (ii) a non-linear transition region to model the uncoiling of fibres; (iii) a stiff quasi-linear region to model fully uncoiled fibres.

The proposed *bilinear* stress-strain relation for the collagen fibres is given as:

$$\sigma_{\text{aniso}} = \sum_{i=4,6} \sigma_{fi} \mathbf{a_i} \otimes \mathbf{a_i},$$
$$\sigma_{fi} = \begin{cases} E_{1f}(\lambda_{fi} - 1) & \lambda_{fi} - 1 \leq D_{1f} \\ p_f(\lambda_{fi} - 1)^2 + q_f(\lambda_{fi} - 1) + r_f & D_{1f} < \lambda_{fi} - 1 < D_{2f} \\ E_{2f}(\lambda_{fi} - 1 - D_{2f}) + (p_f D_{2f}^2 + q_f D_{2f} + r_f) & \lambda_{fi} - 1 \geq D_{2f} \end{cases} \tag{8}$$

where, E_{1f} and E_{2f} are slopes of the linear regimes, D_{1f} and D_{2f} are the values of the nominal fibre strain at the end of the first linear regime and at the beginning of the second linear regime, $\mathbf{a_i}, \mathbf{i} = \mathbf{4}, \mathbf{6}$ are the directions of the fibres in deformed configuration and σ stands for the Cauchy stress. It is noted that the material parameters of the BLF model in equation (8) have a clear physical meaning that can be related to a soft tissue experimental stress-stretch curve. During the initial regime the collagen fibres are tightly coiled. As the initial regime reaches D_{1f} and enters the transition regime the collagen fibres uncoil

which leads to the rapid stiffening of the stress-stretch curve. At D_{2f} , the point where the second linear regime is entered, the collagen fibres are completely uncoiled and behave as straight stiff elastic fibres. Moreover, p_f, q_f and r_f are not independent parameters; in order to maintain C^0 and C^1 continuity the following relations must be enforced:

$$p_f = \frac{E_{1f} - E_{2f}}{2(D_{1f} - D_{2f})}, \quad q_f = E_{1f} - 2D_{1f}p_f, \quad r_f = (E_{1f} - q_f)D_{1f} - p_f D_{1f}^2, \tag{9}$$

The corresponding fibre strain energy density function is given as:

$$\Psi_{\text{aniso}} = \sum_{i=1,2} \Psi_{fi},$$
$$\Psi_{fi} = \begin{cases} E_{1f}(\frac{2}{3}\lambda_{fi}^3 - \lambda_{fi}^2 + \frac{1}{3}) & \lambda_{fi} - 1 \leq D_{1f} \\ \frac{2}{3}\lambda_{fi}^3(q_f - 2p_f) + \frac{p_f}{2}\lambda_{fi}^4 + \lambda_{fi}^2(p_f - q_f + r_f) + \psi_{01} & D_{1f} < \lambda_{fi} - 1 < D_{2f} \\ \frac{2E_{2f}}{3}\lambda_{fi}^3 + \lambda_{fi}^2(p_f D_{2f}^2 + q_f D_{2f} + r_f - E_{2f} - E_{2f}D_{2f}) + \psi_{02} & \lambda_{fi} - 1 \geq D_{2f} \end{cases} \tag{10}$$

where, ψ_{01} and ψ_{02} are two constants which ensure the continuity of strain energy. Figure 4 contains a schematic illustration of the material parameters of the proposed BLF model and functionality of stress and strain energy. An alternative form of the BLF model that uses a single function, rather than the piece-wise function, is presented in Appendix A.

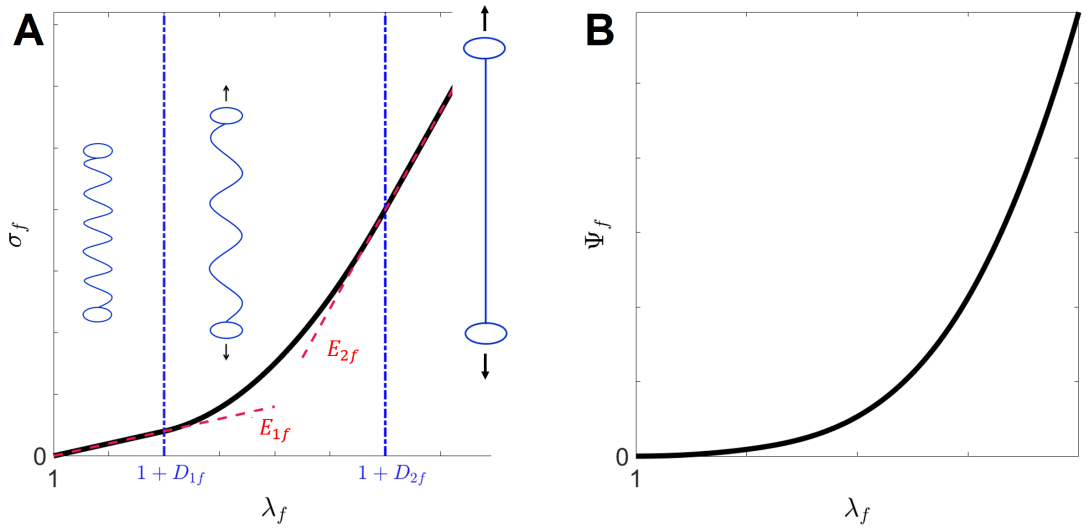

Figure 4: A schematic illustration of a typical σ_f-λ_f (A) and Ψ_f-λ_f (B) curves for the proposed BLF model. The nature of the parameters E_{1f}, D_{1f}, E_{2f} and D_{2f}, and the uncoiling of the collagen fibres during each deformation regime are illustrated. D_{1f} is the nominal strain at the end of the first linear regime which is controlled by the initial slope E_{1f}. D_{2f} is the nominal strain at the beginning of the second linear regime which is controlled by the slope E_{2f}. The low-stiffness and the high-stiffness linear regime are connected by a transition regime between D_{1f} and D_{2f}.

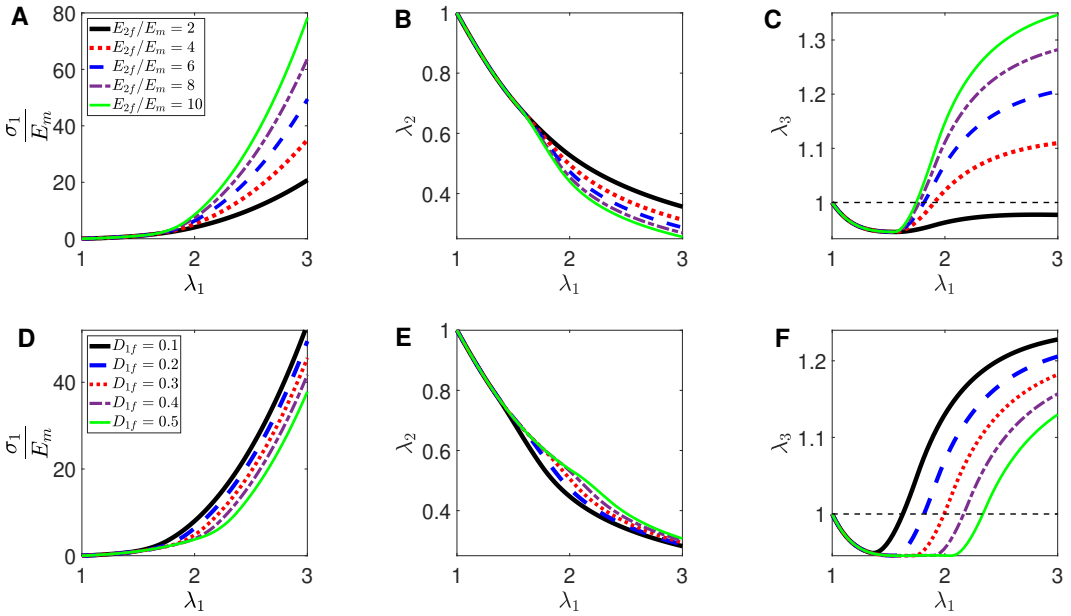

Figure 5: The influence of fibre strain-stiffening and transition strain on the stress (A, D), in-plane transverse stretch (B, E) and out-of-plane stretch (C, F). Reference parameters $E_{1f}/E_m = 1.5$, $\theta = 45^o$, $E_{2f}/E_m = 6$, $D_{1f} = 0.2$, $D_{2f} = D_{1f} + 0.2$ have been used.

The BLF model is placed in parallel with a linear neo-Hookean matrix and subjected

to uniaxial tension boundary conditions. The influence of the fibre strain stiffening in regimes (ii) and (iii) is investigated in Figure 5. In the low-stiffness regime no auxetic behaviour is observed. The onset of fibre strain stiffening in the transition regime leads to an increased rate of compaction in the 2-direction and the onset of auxetic behaviour ($\lambda_3 > 1$). The degree of auxetic deformation increases with increasing fibre strain-stiffening. However, even at low ratios of fibre stiffness to matrix stiffness (e.g. $E_{2f}/E_m = 4$) auxetic deformation occurs upon the onset of fibre strain stiffening. In order to accurately model the anisotropic strain-stiffening behaviour observed in experimental testing of arteries, a high fibre stiffness is required at high strains, so that auxetic behaviour becomes unavoidable if a linear neo-Hookean (constant stiffness) matrix is used. Moreover, increasing the transition strain D_{1f} leads to postponing the auxetic behaviour as it postpones the fibre strain-stiffening (Figure 5 D, E, F). However, it is important to note that the parameters explored in Figure 5 (i.e. the fibre-matrix stiffness ratio (E_{2f}/E_m) and the values of transition strain (e.g. D_{1f} or D_{2f}) are calibrated to fit experimental stress-strain curves, and cannot be arbitrarily chosen to eliminate auxetic behaviour.

5. A strain–stiffening matrix with a strain–stiffening fibre reduces auxetic behaviour

As demonstrated in Figures 3 and 5, auxetic deformation is strongly influenced by the ratio of fibre to matrix stiffness. Auxetic deformation is accentuated by strain-stiffening fibres in a constant stiffness matrix. Therefore, in this section we propose a strain-stiffening isotropic matrix model with near bilinear behaviour (BLM model), placed in parallel with the BLF model described in Section 4. This approach allows precise control of the fibre-matrix stiffness ratio at small and large deformations, facilitating the simulation of anisotropic strain- stiffening behaviour without unphysical auxetic behaviour.

Assuming the isotropic strain energy function $\overline{\Psi}_m(\bar{\lambda}_1, \bar{\lambda}_2, \bar{\lambda}_3)$ for matrix, where $\bar{\lambda}_i, i = 1, 2, 3$ are the modified principal stretches, the Cauchy stress components, σ_i are determined from the following relationship (Holzapfel, 2000):

$$J\sigma_i = \bar{\lambda}_i \frac{\partial \overline{\Psi}_m}{\partial \bar{\lambda}_i} - \frac{1}{3} \sum_{j=1}^{3} \bar{\lambda}_j \frac{\partial \overline{\Psi}_m}{\partial \bar{\lambda}_j}, \qquad i = 1, 2, 3 \tag{11}$$

Using the Valanis-Landel hypothesise the strain energy function $\overline{\Psi}_m(\bar{\lambda}_1, \bar{\lambda}_2, \bar{\lambda}_3)$ is

presented as

$$\overline{\Psi}_m(\bar{\lambda}_1, \bar{\lambda}_2, \bar{\lambda}_3) = \Psi_{iso}(\bar{\lambda}_1) + \Psi_{iso}(\bar{\lambda}_2) + \Psi_{iso}(\bar{\lambda}_3) \tag{12}$$

In order to simulate an isotropic matrix material that exhibits bi-linear type strain-stiffening we propose a isochoric strain energy density function such that:

$$\begin{aligned}\overline{S}_i &= \bar{\lambda}_i \frac{\partial \Psi_{iso}(\bar{\lambda}_i)}{\partial \bar{\lambda}_i} \\ &= \begin{cases} E_{1m}(\bar{\lambda}_i - 1) & |\bar{\lambda}_i - 1| \leq |D_{1m}| \\ p_m(\bar{\lambda}_i - 1)^2 + q_m(\bar{\lambda}_i - 1) + r_m & |D_{1m}| < |\bar{\lambda}_i - 1| < |D_{2m}| \\ E_{2m}(\bar{\lambda}_i - 1 - D_{2m}) + (p_m D_{2m}^2 + q_m D_{2m} + r_m) & |\bar{\lambda}_i - 1| \geq |D_{2m}| \end{cases}\end{aligned} \tag{13}$$

where the parameters E_{1m}, E_{2m}, D_{1m} and D_{2m} have the same meaning as the corresponding parameters in the fibre model (equation (8)) and p_m, q_m, and r_m are obtained in a similar manner as equation (9) by using the corresponding matrix parameters. After a straightforward manipulation the strain energy function associated with equation (13) is obtained as:

$$\Psi_{iso}(\bar{\lambda}_i) =$$

$$\begin{cases} E_{1m}(\bar{\lambda}_i - \ln \bar{\lambda}_i - 1) & |\bar{\lambda}_i - 1| \leq |D_{1m}| \\ p_m(\frac{\bar{\lambda}_i^2}{2} - 2\bar{\lambda}_i + \ln \bar{\lambda}_i) + q_m(\bar{\lambda}_i - \ln \bar{\lambda}_i) + r_m \ln \bar{\lambda}_i + \psi_{01m} & |D_{1m}| < |\lambda_i - 1| < |D_{2m}| \\ E_{2m}(\bar{\lambda}_i - (1 + D_{2m}) \ln \bar{\lambda}_i) + (p_m D_{2m}^2 + q_m D_{2m} + r_m) \ln \bar{\lambda}_i + \psi_{02m} & |\lambda_i - 1| \geq |D_{2m}| \end{cases} \tag{14}$$

where, ψ_{01m} and ψ_{02m} are two constants which ensure the continuity of strain energy. As an alternative formulation to the piece-wise strain-stiffening constitutive law above, we propose a non-piece-wise equivalent formulation in Appendix A (based on error function strain stiffening). It is shown that identical material behaviour can be obtained, both in terms of stress and strain energy density.

This proposed BLM model is used in parallel with our BLF (equation (10)) to investigate the control/elimination of auxetic deformation under uniaxial tension. Henceforth, this combination of matrix and fibre models is called BLFM model for convenience. In Figure 6 we explore the influence of matrix strain-stiffening on auxetic behaviour. Matrix strain-stiffening is characterised by the ratio of the matrix tangent modulus at high strains (E_{2m}) to that at low strains (E_{1m}). Increasing $E_{2m}/E_{1m} > 1$ results in reduced compaction in the 2-direction at higher applied stretch, and consequently a significant reduction in auxetic behaviour. For the parameter sets considered in Figure 6, values of

$\lambda_3 > 1$ are computed only for the case of a non-strain stiffening matrix ($E_{2m}/E_{1m} = 1$). We also explore the influence of the matrix transition strain parameter D_{1m} on auxetic behaviour (with $E_{2m}/E_{1m} = 3$). If the value of D_{1m} is increased, the matrix strain-stiffening is delayed, and may be preceded by significant fibre strain-stiffening. Auxetic behaviour occurs if D_{1m} is significantly higher than D_{1f}. However, if the fibre and the matrix undergo strain-stiffening at similar levels of deformation, auxetic behaviour may be eliminated.

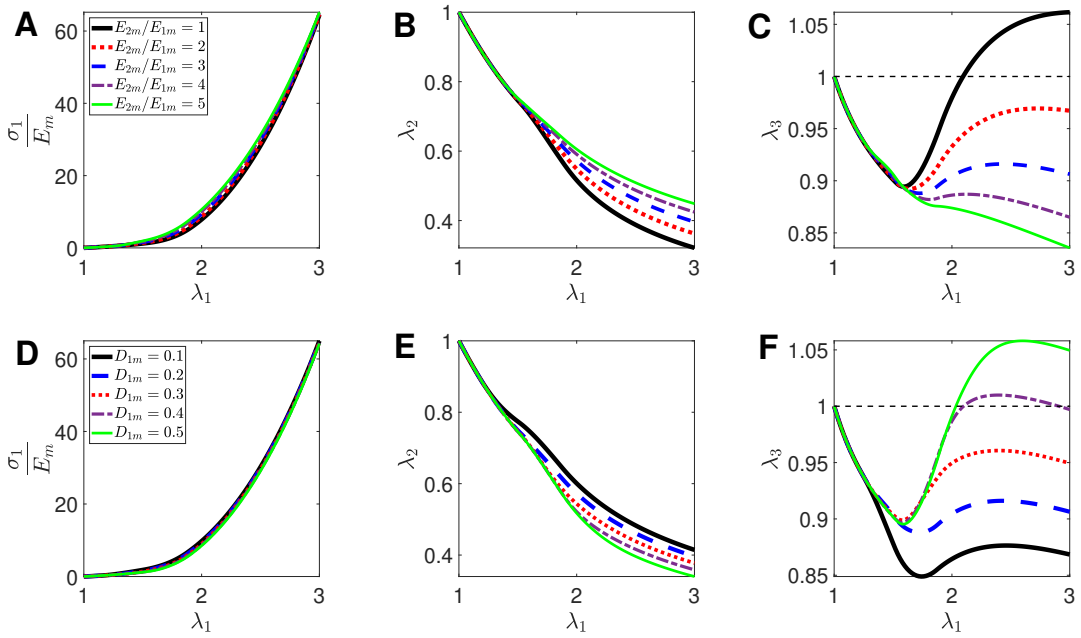

Figure 6: The influence of matrix stiffening and transition strain on the stress (A, D), in-plane transverse stretch (B, E), and auxetic behaviour (C, F). Reference parameters $D_{1f} = 0.2$, $D_{2f} = 0.4$, $E_{1f}/E_{1m} = 1.5$, $\theta = 45^o$, $E_{2f}/E_{1m} = 8$, $D_{1m} = 0.2$, $D_{2m} = D_{1m} + 0.2, E_{2m}/E_{1m} = 3$, $K/E_{1m} = 30$ have been used.

To demonstrate the practical importance of our findings, we use our new fibre/matrix strain-stiffening formulation to simulate experimental test data for aorta tissue (FitzGibbon and McGarry, 2020). The results, as shown in Figure 7, reveal that the BLFM model is not only able to acccurately capture experimentally measured anisotropic stress-stretch data, but also correctly predicts the non-auxetic ($\lambda_3 < 1$) out-of-plane stretch with reasonable accuracy. In contrast, if a non-strain stiffening linear matrix (L-BLF) model is used, significant auxetic behaviour ($\lambda_3 > 1$) is incorrectly computed.

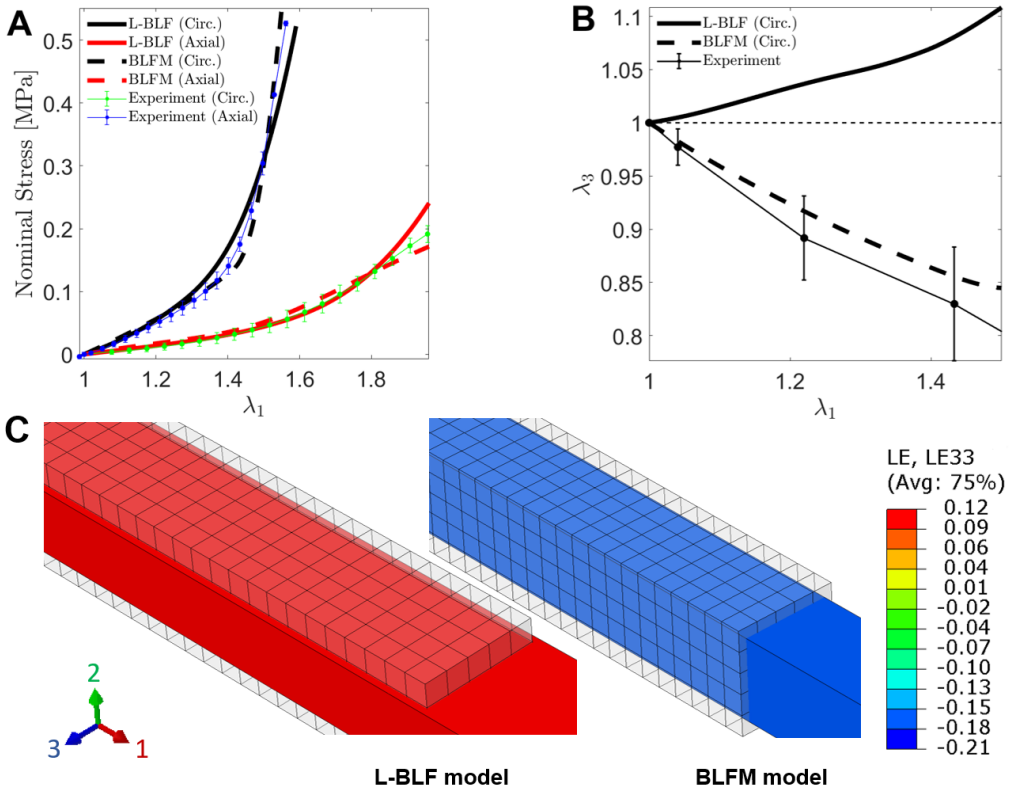

Figure 7: The capability of the BLFM model to reproduce the stress-stretch experimental data of the uniaxial tension of ascending aorta FitzGibbon and McGarry (2020) (A) and out-of-plane stretch in circumferential test (B). FE results of the uniaxial tension tests for BLFM model and L-BLF models are also shown (C). "L-BLF" stands for a linear matrix model in parallel with the BLF model.

6. Auxetic behaviour using an exponentially stiffening fibre model

The strain energy density function for the classical exponential form for collagen fibre strain-stiffening (Holzapfel et al. (2000)), is given as:

$$\Psi_{\text{aniso}}(\mathbf{C}, \mathbf{a}_{04}, \mathbf{a}_{06}) = \frac{k_1}{2k_2} \sum_{i=4,6} \left\{ \exp\left[k_2(I_i - 1)^2\right] \right\} \tag{15}$$

where k_1 and k_2 are material parameters. Note that equation (15) is the modified anisotropic (MA) form for slightly compressible materials ((Nolan et al., 2014)) requiring the use of the full anisotropic invariants $I_{4,6}$ instead of the isochoric anisotropic invariants $\bar{I}_{4,6}$. This exponential fibre component is placed in parallel with a neo-Hookean matrix (equation (6)). This exponential-fibre formulation combined with neo-Hookean matrix has been widely used following implementation in leading commercial FE software programs such

as Abaqus (Abaqus, 2017), FEAP (Taylor, 2013), Ansys (Ansys, 2017) and ADINA (Adina, 2017). It worth to note that although the contribution of the fibres in compression is usually excluded, ANSYS implementation does not include the tension-compression switch of the fibres.

The response to a unixial tension test of this exponential-fibre formulation combined with neo-Hookean matrix is demonstrated in Figure 8 using material parameters calibrated for human coronary arteries (Holzapfel, 2002). Strong strain stiffening and anisotropy is evident in Figure 8A. However, significant auxetic behaviour is evident (Figure 8B), with $\lambda_3 > 1$ when $\lambda_1 > \ 1.15$.

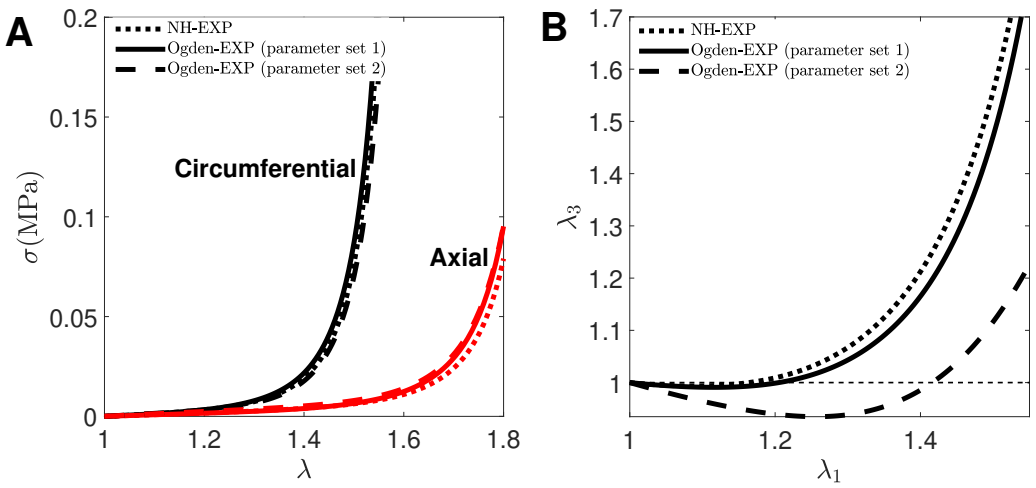

Figure 8: Comparison of Ogden and neo-Hookean matrix in parallel with the exponential fibre model. The combination of Ogden with exponential fibre model postpones the development of auxetic behaviour in comparison to the neo-Hookean matrix with exponential fibre model (B) while the stress-stretch curves are the same for both models (A). The parameters $\mu = 0.0014\,\text{MPa}$, $k_1 = 0.0051\,\text{MPa}$ and $k_2 = 15.4$ have been used for NH-Exp model and two parameter sets (i.e., set 1: $\mu_1 = \mu_2 = 0.0014\,\text{MPa}$, $\alpha_1 = -\alpha_2 = 1.5$, $k_1 = 0.0051\,\text{MPa}$, $k_2 = 15.4$ and set 2: $\mu_1 = \mu_2 = 0.0024\,\text{MPa}$, $\alpha_1 = -\alpha_2 = 4$, $k_1 = 0.0015\,\text{MPa}$, $k_2 = 15.4$) have been used for Ogden-Exp model.

Based on our proposed concept of using a non-linear matrix to control auxetic behaviour (Section 5), here we next explore the combination of the exponential fibre model (equation (15)) with the established Ogden strain-stiffening isotripic hyperelastic model

for the matrix. The Ogden hyperelastic strain energy function is given as:

$$\overline{\Psi}_m(\bar{\lambda}_1, \bar{\lambda}_2, \bar{\lambda}_3) = \sum_{i=1}^{N} \frac{2\mu_i}{\alpha_i^2} \left(\bar{\lambda}_1^{\alpha_i} + \bar{\lambda}_2^{\alpha_i} + \bar{\lambda}_3^{\alpha_i} - 3\right) \tag{16}$$

where, $\bar{\lambda}_1$, $\bar{\lambda}_2$ and $\bar{\lambda}_3$ are isochoric principal stretches and μ_i and α_i are material constants and we assumed $N = 2$ in this paper. Additionally, we retain the isotropic volumetric strain energy density function (first term on RHS of equation (6)) and enforce near incompressibility with $K = 1.4\,\mathrm{MPa}$. The material parameters of the 'Ogden-Exponential' model was chosen to reproduce the anisotropic strain-stiffening behaviour of the aforementioned 'neo-Hookean-Exponential' model (see Figure 8A). Two parameter sets have been found for 'Ogden-Exponential' model which fit the corresponding stress-stain curve of the 'neo-Hookean-Exponential' curve, as shown in Figure 8A. In parameter set 1 a low rate of matrix strain-stiffening is considered. In parameter set 2 a higher rate of matrix strain-stiffening is considered. As shown in Figure 8B, using the Ogden model in place of a neo-Hookean model for the matrix does not eliminate auxetic behaviour, but merely postpones it (in this specific case $\lambda_3 > 1$ when $\lambda_1 > 1.4$.) The stiffness ratio between exponentially stiffening fibres and the power-law stiffening matrix will changes rapidly with increasing applied strain, resulting in uncontrolled auxetic behaviour. In contrast, our proposed BLFM model facilitates control of stiffness ratios and, consequently, elimination of auxetic behaviour.

7. Does including fibre dispersion reduce auxetic behaviour?

In this section the influence of fibre dispersion on auxetic behaviour is investigated. To this end, we have implemented a discrete fibre dispersion method around two mean fibre directions for the exponential (MA) model and the BLF model via the user-defined subroutine UMAT in Abaqus where the mechanical contribution of all fibres under compression are excluded. We consider that fibres can exist in m discrete directions in a 3D sphere at each integration point of a finite element model. A non-uniform segmentation of the unit sphere has been done such that higher density of segmentation around the mean fibre direction is obtained. A sensitivity analysis of the number of fibre directions m revealed that convergence is achieved for $m = 50$.

For each fibre family, the transversely isotropic and π-periodic von-Mises probability distribution function (PDF) ρ_i, as proposed by Gasser et al., (2006), is used to describe

fibre dispersion, whereby

$$\rho_i = \frac{1}{\pi}\sqrt{\frac{b}{2\pi}}\frac{\exp\left[2b(\mathbf{a_{0,i}}.\mathbf{a_{0,mean}})\right]}{\mathrm{erfi}(\sqrt{2b})} \tag{17}$$

where $\mathbf{a_{0,i}}$ is a unit vector indicating one of the m discrete directions, $\mathbf{a_{0,mean}}$ is a unit vector indicating the mean fibre direction, b is a constant dispersion parameter, and $\mathrm{erfi}(x)$ denotes the imaginary error function. The introduction of fibre dispersion results in a fibre contribution in the 3-direction. Therefore, in equation (3), the 33-component of the fibre stress tensor σ_3^f will not be zero, and may therefore influence the computation of auxetic behaviour.

The results for the BLF model and exponential (MA) fibre model, both with a neo-Hookean matrix, are presented in Figure 9.

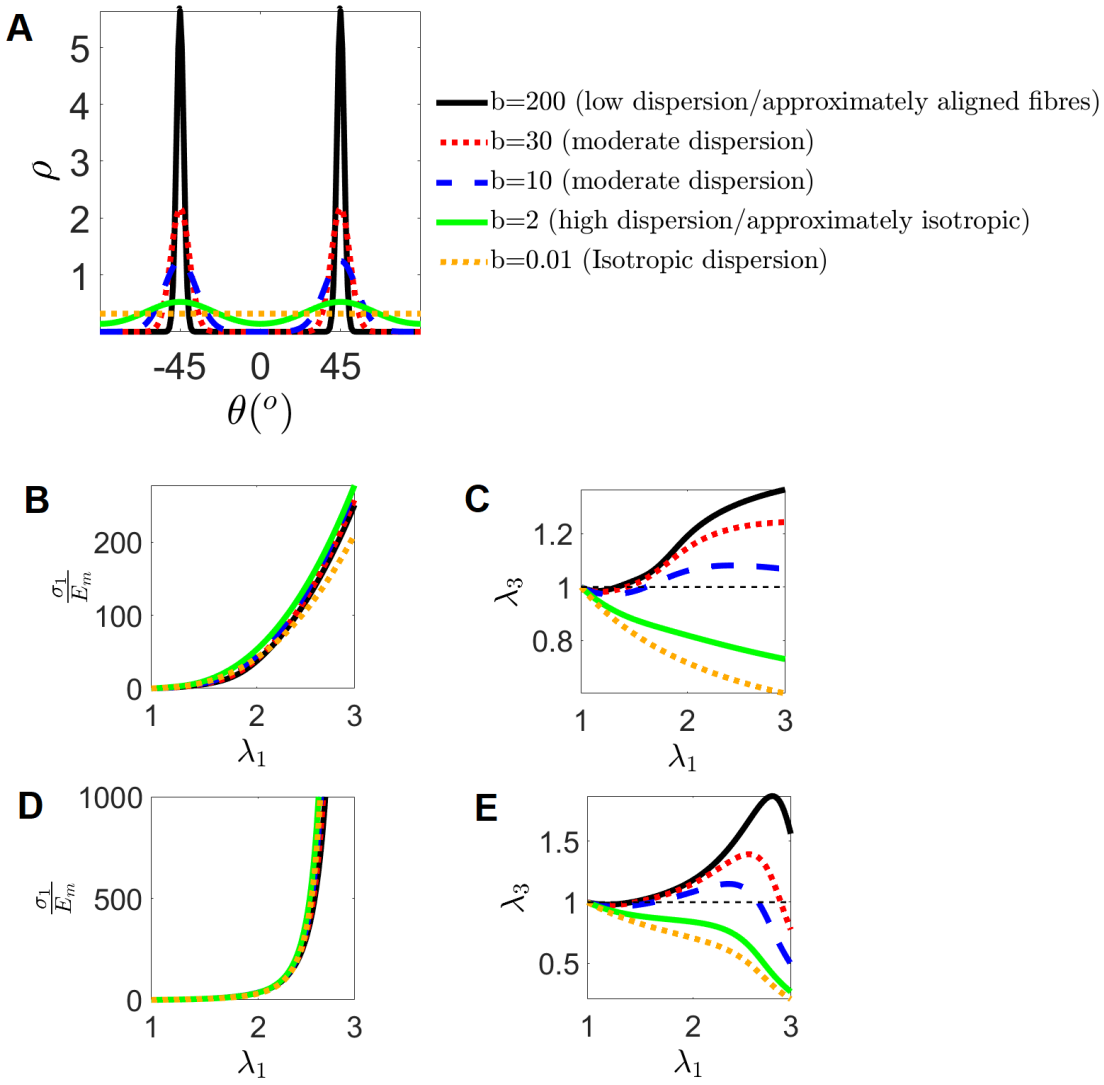

Figure 9: Effects of fibre dispersion on the stress-stretch curve and auxetic behaviour, for bilinear (B,C) and exponential (D,E) fibre models with neo-Hookean model for the matrix. The probability density function, ρ, for the fibres dispersion around the mean fibre directions ($\theta = \pm 45°$) is also shown in (A).

Figure 9 suggests that the inclusion of fibre dispersion does decrease the auxetic deformation in both BLF and exponential MA models. As fibre dispersion is increased the level of auxetic behaviour decreases. However, even for highly dispersed fibres ($b = 10$) auxetic behaviour occurs in both the BLF and exponential MA model. Only in the case of a nearly isotropic fibre distribution (i.e. an isotropic material with nearly equal fibre contribution in all directions) auxetic behaviour is eliminated.

8. Summary and conclusions

In this study we uncover the underlying mechanism of auxetic behaviour in anisotropic hyperelastic soft tissue models that comprise of strain-stiffening fibres in parallel with an isotropic matrix. High levels of in-plane matrix compaction due to increasing tension in strain-stiffening fibres leads to unphysical out-of-plane expansion, i.e. auxetic behaviour. Previous papers have reported the secondary influence of compressibility (Skacel and Bursa, 2016, 2019) and fibre dispersion (Volokh, 2017) on the degree of auxetic behaviour, but no previous study has uncovered this primary underlying mechanism. Furthermore, we propose a new bilinear strain-stiffening fibre and matrix (BLFM) model which facilitates close control of the fibre-matrix stiffness ratio, thereby robustly eliminating auxetic behaviour. We demonstrate that our model provides accurate prediction of experimentally observed out-of-plane compaction, in addition to stress-stretch anisotropy, for arterial tissue subjected to uniaxial tension testing. The key findings of our study are summarised as follows:

- Auxetic deformation is strongly influenced by the ratio of fibre to matrix stiffness.
- Auxetic deformation is accentuated by strain-stiffening fibres in a constant stiffness matrix (e.g., the widely used neo-Hookean matrix with exponentially stiffening fibres).
- Our proposed bilinear strain-stiffening fibre-matrix constitutive model (BLFM model) facilitates robust control of the fibre to matrix stiffness ratio in the low and high deformation regime, consequently eliminating the computation of unphysical auxetic behaviour.
- Our BLFM model is shown to accurately capture experimentally reported anisotropic stress-stretch data for aortic tissue, in addition to correctly predicting the degree of (non-auxetic) compaction in the out-of-plane direction. In contrast, if a non-strain stiffening linear matrix model is used, significant auxetic behaviour is incorrectly computed.

Several studies demonstrate that removal of active cellular contractility, using cytochalasin-D, exposes non-linear strain-stiffening passive behaviour, e.g. (Reynolds et al., 2014;

Reynolds and McGarry, 2015). Therefore, the concept of a strain stiffening matrix introduced in our model may be motivated by the presence of the non-linear passive contribution of endothelial cells, smooth muscle cells, and fibroblasts in arterial tissue, or the passive contribution of cardiac myocytes in cardiac tissue. Of course, the complete description of the non-linear anisotropic behaviour of such tissues requires the addition of our anisotropic fibre component.

The new modelling framework will provide improved predictions of artery deformation during physiological loading and stent deployment without incorrectly predicting auxetic behaviour under such large-strain deformation. Therefore, the new BLFM model can potentially improve current practices in the field of design and regulatory approval of medical devices. Future extensions of the model should consider viscoelasticity (Jacopo and Paola, 2020), viscoplasticity (Weickenmeier and Jabareen, 2014), damage (Fereidoonnezhad et al., 2016; Holzapfel and Fereidoonnezhad, 2017), and non-affine matrix-fibre interaction. The modelling framework should also be considered for anisotropic contractility of smooth muscle cells and fibroblasts (McEvoy et al., 2019), in addition to passive non-linear behaviour of the cell cytoplasm (Reynolds and McGarry, 2015; Weafer et al., 2013). While we specifically calibrate and validate our novel modelling approach using experimental data for aortic tissue, we also explore the ability of our model to robustly eliminate computation unphysical auxetic behaviour over a wide range of applied deformations (including very high deformations that may be encountered for skin (Lanir and Fung, 1974) or urinary bladder samples (Farhat et al., 2008). Future work should precisely calibrate the model using experimental data for several types of soft tissues, including myocardium (McEvoy et al., 2018), cartilage (Dowling et al., 2013) and skin (Annaidh et al., 2012b,a; Limbert, 2019).

Acknowledgements

This work was partially funded by a European Union Horizon 2020 Research and Innovation Program, under grant agreement No. 777072 and Science Foundation Ireland grant number SFI-12/IP/1723.

References

Abaqus, 2017. Analysis user's guide, Dassault Systèmes Simulia Corp. Providence, RI .

Adina, 2017. Adina R&D inc., Watertown, MA, USA.

Annaidh, A.N., Bruyère, K., Destrade, M., Gilchrist, M.D., Maurini, C., Otténio, M., Saccomandi, G., 2012a. Automated estimation of collagen fibre dispersion in the dermis and its contribution to the anisotropic behaviour of skin. Annals of biomedical engineering 40, 1666–1678.

Annaidh, A.N., Bruyère, K., Destrade, M., Gilchrist, M.D., Otténio, M., 2012b. Characterization of the anisotropic mechanical properties of excised human skin. Journal of the mechanical behavior of biomedical materials 5, 139–148.

Ansys, 2017. Ansys inc., Canonsburg, PA, USA., www.ansys.com.

Brown, C., Nguyen, T., Moody, H., Crawford, R., Oloyede, A., 2009. Assessment of common hyperelastic constitutive equations for describing normal and osteoarthritic articular cartilage. Proceedings of the Institution of Mechanical Engineers, Part H: Journal of Engineering in Medicine 223, 643–652.

Deneweth, J.M., Arruda, E.M., McLean, S.G., 2015. Hyperelastic modeling of location-dependent human distal femoral cartilage mechanics. International Journal of Non-Linear Mechanics 68, 146–156.

Dowling, E.P., Ronan, W., McGarry, J.P., 2013. Computational investigation of in situ chondrocyte deformation and actin cytoskeleton remodelling under physiological loading. Acta biomaterialia 9, 5943–5955.

Farhat, W.A., Chen, J., Haig, J., Antoon, R., Litman, J., Sherman, C., Derwin, K., Yeger, H., 2008. Porcine bladder acellular matrix (acm): protein expression, mechanical properties. Biomedical Materials 3, 025015.

Fereidoonnezhad, B., Naghdabadi, R., Holzapfel, G., 2016. Stress softening and permanent deformation in human aortas: continuum and computational modeling with application to arterial clamping. Journal of the mechanical behavior of biomedical materials 61, 600–616.

Fereidoonnezhad, B., Naghdabadi, R., Sohrabpour, S., Holzapfel, G., 2017. A mechanobiological model for damage-induced growth in arterial tissue with application to in-stent restenosis. Journal of the Mechanics and Physics of Solids 101, 311–327.

FitzGibbon, B., McGarry, P., 2020. Development of a novel test method to investigate mode II fracture and dissection of arteries. https://doi.org/10.31224/osf.io/d3jbr. doi:10.31224/osf.io/d3jbr.

Gasser, T.C., Gallinetti, S., Xing, X., Forsell, C., Swedenborg, J., Roy, J., 2012. Spatial orientation of collagen fibers in the abdominal aortic aneurysm's wall and its relation to wall mechanics. Acta biomaterialia 8, 3091–3103.

Gasser, T.C., Ogden, R.W., Holzapfel, G.A., 2006. Hyperelastic modelling of arterial layers with distributed collagen fibre orientations. Journal of the royal society interface 3, 15–35.

Guo, Z., Peng, X., Moran, B., 2006. A composites-based hyperelastic constitutive model for soft tissue with application to the human annulus fibrosus. Journal of the Mechanics and Physics of Solids 54, 1952–1971.

Holzapfel, A.G., 2000. Nonlinear solid mechanics II. John Wiley & Sons, Inc.

Holzapfel, G.A., 2002. Biomechanics of soft tissues with application to arterial walls. Mathematical and computational modeling of biological systems , 1–37.

Holzapfel, G.A., Fereidoonnezhad, B., 2017. Modeling of damage in soft biological tissues, in: Biomechanics of Living Organs. Elsevier, pp. 101–123.

Holzapfel, G.A., Gasser, T.C., Ogden, R.W., 2000. A new constitutive framework for arterial wall mechanics and a comparative study of material models. Journal of elasticity and the physical science of solids 61, 1–48.

Holzapfel, G.A., Niestrawska, J.A., Ogden, R.W., Reinisch, A.J., Schriefl, A.J., 2015. Modelling non-symmetric collagen fibre dispersion in arterial walls. Journal of the Royal Society Interface 12, 20150188.

Holzapfel, G.A., Ogden, R.W., 2017. On fiber dispersion models: exclusion of compressed fibers and spurious model comparisons. Journal of elasticity 129, 49–68.

Jacopo, C., Paola, N., 2020. A structurally frame-indifferent model for anisotropic visco-hyperelastic materials. arXiv preprint arXiv:2006.08744 .

Lanir, Y., Fung, Y., 1974. Two-dimensional mechanical properties of rabbit skin—ii. experimental results. Journal of biomechanics 7, 171–182.

Lim, T.C., 2015. Auxetic materials and structures. Springer.

Limbert, G., 2019. Skin Biophysics: From Experimental Characterisation to Advanced Modelling. volume 22. Springer.

McEvoy, E., Deshpande, V.S., McGarry, P., 2019. Transient active force generation and stress fibre remodelling in cells under cyclic loading. Biomechanics and modeling in mechanobiology 18, 921–937.

McEvoy, E., Holzapfel, G.A., McGarry, P., 2018. Compressibility and anisotropy of the ventricular myocardium: experimental analysis and microstructural modeling. Journal of biomechanical engineering 140.

Moerman, K.M., Fereidoonnezhad, B., McGarry, J.P., 2020. Novel hyperelastic models for large volumetric deformations. International Journal of Solids and Structures 193, 474–491.

Nolan, D., Gower, A., Destrade, M., Ogden, R., McGarry, J., 2014. A robust anisotropic hyperelastic formulation for the modelling of soft tissue. Journal of the mechanical behavior of biomedical materials 39, 48–60.

Nolan, D., McGarry, J., 2016a. On the compressibility of arterial tissue. Annals of biomedical engineering 44, 993–1007.

Nolan, D., McGarry, J., 2016b. On the compressibility of arterial tissue. Annals of biomedical engineering 44, 993–1007.

Peng, X., Guo, Z., Moran, B., 2006. An anisotropic hyperelastic constitutive model with fiber-matrix shear interaction for the human annulus fibrosus. Journal of Applied Mechanics .

Pierce, D.M., Ricken, T., Holzapfel, G.A., 2013. A hyperelastic biphasic fibre-reinforced model of articular cartilage considering distributed collagen fibre orientations: continuum basis, computational aspects and applications. Computer methods in biomechanics and biomedical engineering 16, 1344–1361.

Reynolds, N., McGarry, J., 2015. Single cell active force generation under dynamic loading–part ii: Active modelling insights. Acta Biomaterialia 27, 251–263.

Reynolds, N.H., Ronan, W., Dowling, E.P., Owens, P., McMeeking, R.M., McGarry, J.P., 2014. On the role of the actin cytoskeleton and nucleus in the biomechanical response of spread cells. Biomaterials 35, 4015–4025.

Skacel, P., Bursa, J., 2016. Poisson's ratio of arterial wall–inconsistency of constitutive models with experimental data. Journal of the mechanical behavior of biomedical materials 54, 316–327.

Skacel, P., Bursa, J., 2019. Compressibility of arterial wall–direct measurement and predictions of compressible constitutive models. Journal of the mechanical behavior of biomedical materials 90, 538–546.

Taylor, R., 2013. Feap- a finite element analysis program, version 8.4, user manual, department of civil and environmental engineering. University of California at Berkeley, Berkeley .

Volokh, K.Y., 2017. On arterial fiber dispersion and auxetic effect. Journal of biomechanics 61, 123–130.

Weafer, P., Ronan, W., Jarvis, S., McGarry, J., 2013. Experimental and computational investigation of the role of stress fiber contractility in the resistance of osteoblasts to compression. Bulletin of mathematical biology 75, 1284–1303.

Weickenmeier, J., Jabareen, M., 2014. Elastic–viscoplastic modeling of soft biological tissues using a mixed finite element formulation based on the relative deformation gradient. International journal for numerical methods in biomedical engineering 30, 1238–1262.

Appendix A.

An alternative non–piece-wise constitutive formulation is proposed in this appendix. This formulation uses error functions to describe transition from low stiffness to the high stiffness regimes. First, we propose the following form for the derivative of the stress term $\overline{S}_i$:

$$\begin{aligned} \frac{d\overline{S}_i}{d\bar{\lambda}_i} &= \frac{d}{d\bar{\lambda}_i}\left(\bar{\lambda}_i \frac{d\Psi_{iso}(\bar{\lambda}_i)}{d\bar{\lambda}_i}\right) = B_t + A_t f_t(\bar{\lambda}_i) + B_c + A_c f_c(\bar{\lambda}_i), \\ f_t(\bar{\lambda}_i) &= \mathrm{erf}\big(\frac{\bar{\lambda}_i - a_t}{b_t}\big), \quad f_c(\bar{\lambda}_i) = \mathrm{erf}\big(\frac{\bar{\lambda}_i - a_c}{b_c}\big) \end{aligned} \tag{A.1}$$

in which, the following parameters are introduced:

$$\begin{aligned} A_t &= \frac{E^t_{2m} - E_{1m}}{f_t(1+D^t_{2m}) - f_t(1+D^t_{1m})}, \qquad B_t = \frac{E_{1m}}{2} - A_t f_t(1+D^t_{1m}). \\ a_t &= 1 + \frac{D^t_{2m} + D^t_{1m}}{2}, \qquad b_t = \frac{\sqrt{2}}{\beta_m}(D^t_{2m} - D^t_{1m}) \\ A_c &= \frac{E^c_{2m} - E_{1m}}{f_c(1+D^c_{2m}) - f_c(1+D^c_{1m})}, \qquad B_c = \frac{E_{1m}}{2} - A_c f_c(1+D^c_{1m}). \\ a_c &= 1 + \frac{D^c_{2m} + D^c_{1m}}{2}, \qquad b_c = \frac{\sqrt{2}}{\beta_m}(D^c_{2m} - D^c_{1m}) \end{aligned} \tag{A.2}$$

To enforce symmetric tension–compression matrix behaviour in terms of Cauchy stress, the following relationship between parameters should be maintained:

$$D^c_{1m} = -D^c_{1m} = D_{1m}, \quad D^c_{2m} = -D^c_{2m} = D_{2m}, \quad E^t_{2m} = E^c_{2m} = E_{2m} \tag{A.3}$$

where, the material parameters D_{1m}, D_{2m}, E_{1m}, and E_{2m} have the same meaning as the corresponding parameters in Equation (13). Moreover, to get a monotonic transition from the low stiffness region to the high stiffness region, same as the piece-wise formulation, the value of parameter β_m should be chosen in the range of $5 \leq \beta_m \leq 10$. Integrating equation (A.1) results in the following:

$$\begin{aligned} \overline{S}_i &= \bar{\lambda}_i \frac{d\Psi_{iso}(\bar{\lambda}_i)}{d\bar{\lambda}_i} = \int \big(B_t + A_t f_t(\bar{\lambda}_i) + B_c + A_c f_c(\bar{\lambda}_i)\big) d\bar{\lambda}_i \\ &= B_t\bar{\lambda}_i + \frac{A_t b_t}{\sqrt{\pi}}\exp\big(-\frac{(\bar{\lambda}_i - a_t)^2}{b_t^2}\big) + A_t(\bar{\lambda}_i - a_t)\mathrm{erf}\big(\frac{\bar{\lambda}_i - a_t}{b_t}\big) \\ &+ B_c\bar{\lambda}_i + \frac{A_c b_c}{\sqrt{\pi}}\exp\big(-\frac{(\bar{\lambda}_i - a_c)^2}{b_c^2}\big) + A_c(\bar{\lambda}_i - a_c)\mathrm{erf}\big(\frac{\bar{\lambda}_i - a_c}{b_c}\big) + c_1 \end{aligned} \tag{A.4}$$

where the integration constant c_1 is obtained from the condition that the material is stress-free in the undeformed configuration, i.e.,

$$\begin{aligned}
&\left(\bar{\lambda}_i \frac{d\Psi_{iso}(\bar{\lambda}_i)}{d\bar{\lambda}_i}\right)_{\bar{\lambda}_i=1} = 0 \rightarrow \\
c_1 = &-A_t \frac{b_t}{\sqrt{\pi}} \exp\left(-\frac{(1-a_t)^2}{b_t^2}\right) - A_t(1-a_t)\mathrm{erf}\left(\frac{1-a_t}{b_t}\right) - B_t \\
&- A_c \frac{b_c}{\sqrt{\pi}} \exp\left(-\frac{(1-a_c)^2}{b_c^2}\right) - A_c(1-a_c)\mathrm{erf}\left(\frac{1-a_c}{b_c}\right) - B_c
\end{aligned} \tag{A.5}$$

Integrating equation (A.4) is then results in

$$\begin{aligned}
\Psi_{iso}(\bar{\lambda}_i) = &(B_t + B_c)\bar{\lambda}_i + c_1 \ln \bar{\lambda}_i \\
&+ \frac{A_t b_t}{\sqrt{\pi}} \int \frac{1}{\bar{\lambda}_i} \exp\Big(-\frac{(\bar{\lambda}_i - a_t)^2}{b_t^2}\Big) d\bar{\lambda}_i + A_t \int \mathrm{erf}\Big(\frac{\bar{\lambda}_i - a_t}{b_t}\Big) d\bar{\lambda}_i \\
&- A_t a_t \int \frac{1}{\bar{\lambda}_i} \mathrm{erf}\Big(\frac{\bar{\lambda}_i - a_t}{b_t}\Big) d\bar{\lambda}_i + \frac{A_c b_c}{\sqrt{\pi}} \int \frac{1}{\bar{\lambda}_i} \exp\Big(-\frac{(\bar{\lambda}_i - a_c)^2}{b_c^2}\Big) d\bar{\lambda}_i \\
&+ A_c \int \mathrm{erf}\Big(\frac{\bar{\lambda}_i - a_c}{b_c}\Big) d\bar{\lambda}_i - A_c a_c \int \frac{1}{\bar{\lambda}_i} \mathrm{erf}\Big(\frac{\bar{\lambda}_i - a_c}{b_c}\Big) d\bar{\lambda}_i
\end{aligned} \tag{A.6}$$

The integrals in equation(A.6) are then computed as:

$$\begin{aligned}
\int \mathrm{erf}\Big(\frac{\bar{\lambda}_i - a_t}{b_t}\Big) d\bar{\lambda}_i &= \frac{b_t}{\sqrt{\pi}} \exp\left(-\frac{(\bar{\lambda}_i - a_t)^2}{b_t^2}\right) + (\bar{\lambda}_i - a_t)\mathrm{erf}\Big(\frac{\bar{\lambda}_i - a_t}{b_t}\Big), \\
\int \mathrm{erf}\Big(\frac{\bar{\lambda}_i - a_c}{b_c}\Big) d\bar{\lambda}_i &= \frac{b_c}{\sqrt{\pi}} \exp\left(-\frac{(\bar{\lambda}_i - a_c)^2}{b_c^2}\right) + (\bar{\lambda}_i - a_c)\mathrm{erf}\Big(\frac{\bar{\lambda}_i - a_c}{b_c}\Big).
\end{aligned} \tag{A.7}$$

Moreover, by choosing $z_t = \dfrac{\bar{\lambda}_i - a_t}{b_t}, z_c = \dfrac{\bar{\lambda}_i - a_c}{b_c}$, and integrating by part, other integrals in the RHS of equation (A.6) can be expressed as:

$$\begin{aligned}
&\int \frac{1}{\bar{\lambda}_i} \mathrm{erf}\Big(\frac{\bar{\lambda}_i - a_t}{b_t}\Big) d\bar{\lambda}_i = \int \frac{1}{z_t + \frac{a_t}{b_t}} \mathrm{erf}(z_t) dz_t \\
&= \mathrm{erf}(z_t) \ln\left(z_t + \frac{a_t}{b_t}\right) - \frac{2}{\sqrt{\pi}} \int \ln\left(z_t + \frac{a_t}{b_t}\right) \exp\left(-z_t^2\right) dz_t, \\
&\int \frac{1}{\bar{\lambda}_i} \mathrm{erf}\Big(\frac{\bar{\lambda}_i - a_c}{b_c}\Big) d\bar{\lambda}_i = \int \frac{1}{z_c + \frac{a_c}{b_c}} \mathrm{erf}(z_c) dz_c \\
&= \mathrm{erf}(z_c) \ln\left(z_c + \frac{a_c}{b_c}\right) - \frac{2}{\sqrt{\pi}} \int \ln\left(z_c + \frac{a_c}{b_c}\right) \exp\left(-z_c^2\right) dz_c,
\end{aligned} \tag{A.8}$$

and,

$$\begin{aligned}
&\int \frac{1}{\bar{\lambda}_i} \exp\Big(-\frac{(\bar{\lambda}_i - a_t)^2}{b_t^2}\Big) d\bar{\lambda}_i = \int \frac{1}{z_t + \frac{a_t}{b_t}} \exp(-z_t^2) dz_t \\
&= \exp(-z_t^2) \ln\left(z_t + \frac{a_t}{b_t}\right) + \int 2z_t \ln\left(z_t + \frac{a_t}{b_t}\right) \exp\left(-z_t^2\right) dz_t \\
&\int \frac{1}{\bar{\lambda}_i} \exp\Big(-\frac{(\bar{\lambda}_i - a_c)^2}{b_c^2}\Big) d\bar{\lambda}_i = \int \frac{1}{z_c + \frac{a_t}{b_c}} \exp(-z_c^2) dz_c \\
&= \exp(-z_c^2) \ln\left(z_c + \frac{a_c}{b_c}\right) + \int 2z_c \ln\left(z_c + \frac{a_c}{b_c}\right) \exp\left(-z_c^2\right) dz_c.
\end{aligned} \tag{A.9}$$

Substituting equations (A.7)-(A.9) into equation (A.6), the strain energy density function, Ψ_{iso}, is obtained as:

$$\begin{aligned}\Psi_{iso}(\bar{\lambda}_i) &= (B_t + B_c)\bar{\lambda}_i + c_3 \ln \bar{\lambda}_i \\ &+ \frac{A_t b_t}{\sqrt{\pi}} \left(\exp(-z_t^2)(\ln (z_t + \frac{a_t}{b_t}) + 1) \right) \\ &+ A_t \left((\bar{\lambda}_i - a_t)\mathrm{erf}(\frac{\bar{\lambda}_i - a_t}{b_t}) - a_t \,\mathrm{erf}(z_t) \ln (z_t + \frac{a_t}{b_t}) \right) \\ &+ \frac{2A_t}{\sqrt{\pi}} \int (a_t + b_t z_t) \ln (z_t + \frac{a_t}{b_t}) \exp (-z_t^2) dz_t \\ &+ \frac{A_c b_c}{\sqrt{\pi}} \left(\exp(-z_c^2)(\ln (z_c + \frac{a_c}{b_c}) + 1) \right) \\ &+ A_c \left((\bar{\lambda}_i - a_c)\mathrm{erf}(\frac{\bar{\lambda}_i - a_c}{b_c}) - a_c \,\mathrm{erf}(z_c) \ln (z_c + \frac{a_c}{b_c}) \right) \\ &+ \frac{2A_c}{\sqrt{\pi}} \int (a_c + b_c z_c) \ln (z_c + \frac{a_c}{b_c}) \exp (-z_c^2) dz_c + \psi_{0m}\end{aligned} \tag{A.10}$$

where the constant value ψ_{0m} ensures that the strain energy function $\Psi_{iso}(\bar{\lambda}_i)$ is zero in the undeformed configuration ($\bar{\lambda}_i = 1$). Finally, substituting $z_t = \dfrac{\bar{\lambda}_i - a_t}{b_t}, z_c = \dfrac{\bar{\lambda}_i - a_c}{b_c}$ in equation (A.10) results in:

$$\begin{aligned}\Psi_{iso}(\bar{\lambda}_i) &= (B_t + B_c)\bar{\lambda}_i + c_3 \ln \bar{\lambda}_i \\ &+ \frac{A_t b_t}{\sqrt{\pi}} \left[\exp \left(-\frac{(\bar{\lambda}_i - a_t)^2}{b_t^2} \right) \left(\ln (\frac{\bar{\lambda}_i}{b_t}) + 1 \right) \right] \\ &+ A_t \left((\bar{\lambda}_i - a_t)\mathrm{erf}(\frac{\bar{\lambda}_i - a_t}{b_t}) - a_t \,\mathrm{erf}(\frac{\bar{\lambda}_i - a_t}{b_t}) \ln (\frac{\bar{\lambda}_i}{b_t}) \right) \\ &+ \frac{2A_t}{\sqrt{\pi} b_t} \int \bar{\lambda}_i \ln (\frac{\bar{\lambda}_i}{b_t}) \exp \left(-\frac{(\bar{\lambda}_i - a_t)^2}{b_t^2} \right) d\bar{\lambda}_i \\ &+ \frac{A_c b_c}{\sqrt{\pi}} \left[\exp \left(-\frac{(\bar{\lambda}_i - a_c)^2}{b_c^2} \right) \left(\ln (\frac{\bar{\lambda}_i}{b_c}) + 1 \right) \right] \\ &+ A_c \left((\bar{\lambda}_i - a_c)\mathrm{erf}(\frac{\bar{\lambda}_i - a_c}{b_c}) - a_c \,\mathrm{erf}(\frac{\bar{\lambda}_i - a_c}{b_c}) \ln (\frac{\bar{\lambda}_i}{b_c}) \right) \\ &+ \frac{2A_c}{\sqrt{\pi} b_c} \int \bar{\lambda}_i \ln (\frac{\bar{\lambda}_i}{b_c}) \exp \left(-\frac{(\bar{\lambda}_i - a_c)^2}{b_c^2} \right) d\bar{\lambda}_i + \psi_{0m}\end{aligned} \tag{A.11}$$

This error function based formulation can, of course, also be used for the fibre strain energy function rather than the piece-wise formulation (10). In Figure A1 we demonstrate that the piece-wise formulation (14) and the alternative error function based formulation (A.11) give identical results in terms of matrix stress and strain energy density function.

However, it should be noted that the piece-wise formulation has a simpler closed–form solution for the strain energy density function compared to the error function model. Therefore, we suggest that the piece-wise formulation is more convenient when calculation of the strain energy density function is required (in addition to the calculation of the stress), e.g., in energy-based damage models (Holzapfel and Fereidoonnezhad, 2017; Fereidoonnezhad et al., 2017).

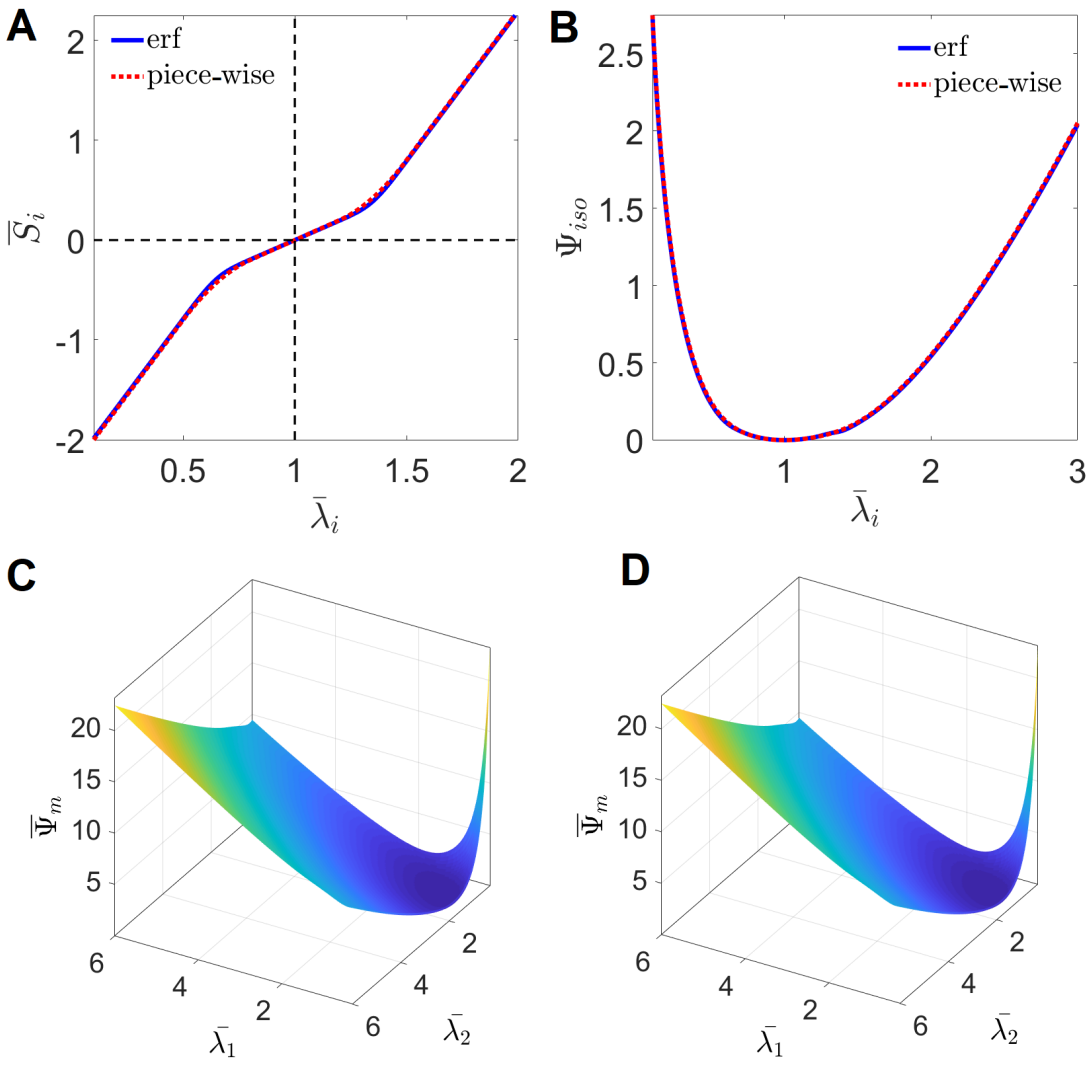

Figure A1: Comparison of the two proposed strain-stiffening models for matrix in tension and compression; (A) Stress-stretch, (B) strain energy density function, (C) the strain energy density surface for the error function formulation (equation (A.11)), and (D) the strain energy density surface for the piece-wise formulation (equation (14)). The material parameters of $D_{1m} = 0.2$, $D_{2m} = 0.5$, $E_{1m} = 1$, $E_{2m} = 3$, and $\beta_m = 5$ have been used.